JACS
JOURNAL OF THE AMERICAN CHEMICAL SOCIETY

Article

pubs.acs.org/JACS

Gold Nanoparticles Located at the Interface of Anatase/Rutile TiO_2 Particles as Active Plasmonic Photocatalysts for Aerobic Oxidation

Daijiro Tsukamoto,† Yasuhiro Shiraishi,*,† Yoshitsune Sugano,† Satoshi Ichikawa,‡ Shunsuke Tanaka,§ and Takayuki Hirai†

†Research Center for Solar Energy Chemistry and Division of Chemical Engineering, Graduate School of Engineering Science, Osaka University, Toyonaka 560-8531, Japan

‡Institute for NanoScience Design, Osaka University, Toyonaka 560-8531, Japan

§Department of Chemical, Energy and Environmental Engineering, Kansai University, Suita 564-8680, Japan

Supporting Information

ABSTRACT: Visible-light irradiation ($\lambda > 450$ nm) of gold nanoparticles loaded on a mixture of anatase/rutile TiO_2 particles (Degussa, P25) promotes efficient aerobic oxidation at room temperature. The photocatalytic activity critically depends on the catalyst architecture: Au particles with <5 nm diameter located at the interface of anatase/rutile TiO_2 particles behave as the active sites for reaction. This photocatalysis is promoted via plasmon activation of the Au particles by visible light followed by consecutive electron transfer in the Au/rutile/anatase contact site. The activated Au particles transfer their conduction electrons to rutile and then to adjacent anatase TiO_2. This catalyzes the oxidation of substrates by the positively charged Au particles along with reduction of O_2 by the conduction band electrons on the surface of anatase TiO_2. This plasmonic photocatalysis is successfully promoted by sunlight exposure and enables efficient and selective aerobic oxidation of alcohols at ambient temperature.

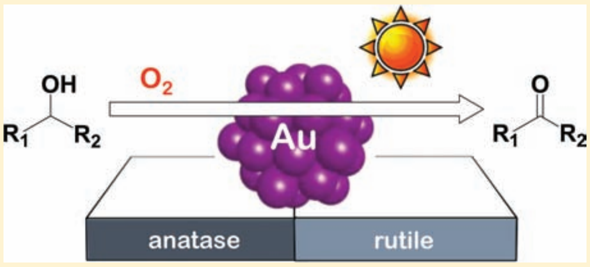

INTRODUCTION

Gold nanoparticles on solid supports have been extensively studied as promising heterogeneous catalysts for a variety of oxidation reactions. In particular, aerobic oxidation with O_2 as an oxidant has attracted a great deal of attention from the viewpoint of green chemistry.[1−4] Several types of substrates, such as alcohols,[4−9] aldehydes,[10] and hydrocarbons,[11,12] are successfully oxidized at ∼393 K by Au particles on neutral supports such as TiO_2 or basic supports such as CeO_2. Extensive studies have revealed that the size of Au particles is critical for their catalytic activity; Au particles with a diameter (d_{Au}) of 2−5 nm show especially high activity for oxidation of CO and propylene.[13−15]

The application of Au particles to optical materials for biological imaging/sensing has also attracted much attention because of their strong light absorption in the visible region, which arises from a resonant oscillation of free electrons coupled by light, known as localized surface plasmon resonance (SPR).[16] The application of SPR to photovoltaic cells has also been studied for light-to-energy conversion. Tian et al.[17] reported that visible-light irradiation ($\lambda > 420$ nm) of Au particles on a semiconductor TiO_2 film coated on an indium tin oxide electrode generates an anodic photocurrent in the presence of Fe^{2+}. This photoelectrochemical response is explained by an electron transfer mechanism similar to that for dye-sensitized TiO_2:[18] collective oscillation of electrons on the Au particles induced by the incident light transfers conduction electrons (e^-) from the Au particles to the TiO_2 conduction band, and the positively charged Au particles receive e^- from the electron donor (Fe^{2+}).

This e^- transfer implies that, as depicted in Scheme 1, plasmon activation of Au particles on semiconductor particles by visible light generates positive charges on the Au particles and conduction-band e^- on the semiconductor particles. This means that oxidation and reduction reactions occur simultaneously, as with conventional semiconductor catalysts activated

Scheme 1. Proposed Mechanism for Visible-Light-Driven Aerobic Oxidation by Au Particles Supported on Semiconductor Particles

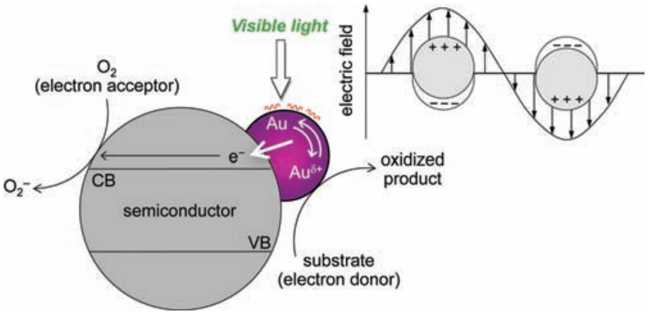

Received: December 26, 2011
Published: March 22, 2012

by UV light.[19] This plasmonic photocatalyst, if employed for aerobic oxidation, might oxidize a substrate (electron donor) on the Au surface, while e^- is consumed by the reduction of O_2 (electron acceptor) on the semiconductor surface. This may promote aerobic oxidation at room temperature under sunlight irradiation,[20] enabling green organic transformations.

This scenario has motivated the application of plasmonic photocatalysis to aerobic oxidation. Kowalska et al.[21] studied the activity of Au particles (d_{Au} = 12−60 nm) loaded on TiO_2 for aerobic oxidation of 2-propanol at room temperature under visible-light irradiation ($\lambda > 450$ nm). They reported that while no reaction occurs in the dark, visible-light irradiation produces acetone and larger Au particles loaded on rutile TiO_2 show better catalytic activity. Tanaka et al.[22] studied aerobic oxidation of benzylic alcohols with Au particles (d_{Au} = 13−70 nm) loaded on CeO_2 at room temperature under irradiation with green light (λ_{max} = 530 nm). They also found that while no reaction occurs in the dark, light irradiation produces benzaldehyde and larger Au particles ($d_{Au} > 30$ nm) show better activity. These studies, however, did not take into consideration the size dependence of the catalytic activity of Au particles for aerobic oxidation in the dark;[13−15] small Au particles ($d_{Au} < 5$ nm) are active, but large ones are inactive. This means that in the above reports,[21,22] the photoreaction was carried out using catalysts with inherently low activity in the dark; therefore, it is unclear whether the photoreaction is actually advantageous over the dark reaction.

Herein we report an active plasmonic photocatalyst that definitely shows enhanced activity relative to the reaction in the dark at room temperature. The catalyst architecture is critical for the activity: small Au particles ($d_{Au} < 5$ nm) loaded on a mixture of anatase/rutile TiO_2 particles (Degussa, P25) are necessary. The place where the Au particles are loaded is also important: Au particles located at the anatase/rutile interface behave as the active sites, facilitating efficient e^- transfer to TiO_2 and successful aerobic oxidation under irradiation with sunlight.

■ RESULTS AND DISCUSSION

Catalyst Preparation. Au/TiO_2 catalysts were prepared by a deposition−precipitation (DP) method[13,15] using anatase (Japan Reference Catalyst JRC-TIO-1; average particle size, 21 nm; BET surface area, 80 $m^2\ g^{-1}$), rutile (JRC-TIO-6; 15 nm; 104 $m^2\ g^{-1}$), and P25 (JRC-TIO-4; 24 nm; 57 $m^2\ g^{-1}$; anatase/rutile ≈ 83/17) TiO_2, which were supplied by the Catalyst Society of Japan. The respective TiO_2 particles were stirred in water (pH 7) with $HAuCl_4$ at 353 K and calcined in air at 473−873 K, affording purple powders of $Au_x(DP_y)/TiO_2$, where x is the amount (in wt %) of Au loaded [x wt % = Au/(Au + TiO_2) × 100%] and y is the calcination temperature (in K). The transmission electron microscopy (TEM) images of the catalysts show hemispherical Au particles (Figure S1 in the Supporting formation). The average diameters of the Au particles on the $Au_2(DP_{673})$/anatase, $Au_2(DP_{673})$/rutile, and $Au_2(DP_{673})$/P25 catalysts are d_{Au} = 4.6, 4.2, and 3.7 nm, respectively. Diffuse-reflectance UV−vis spectra of the catalysts (Figure 1a) show a strong absorption band at ca. 550 nm assigned to the SPR of the Au particles.[20]

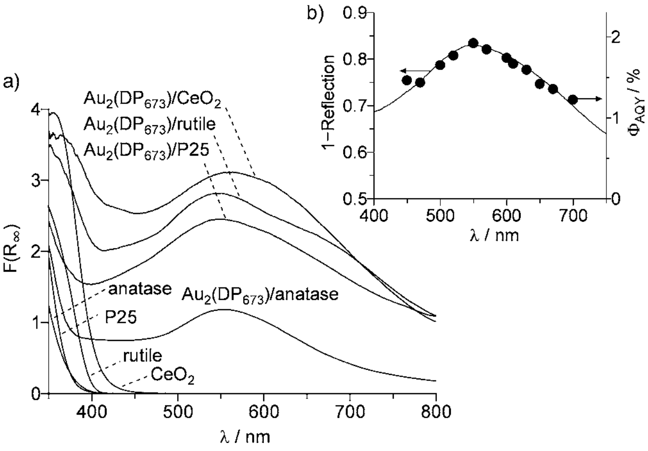

Figure 1. (a) Diffuse reflectance UV−vis spectra of the catalysts. The spectra for other catalysts are summarized in Figure S2 in the Supporting Information. (b) Action spectrum for aerobic oxidation of **1** on $Au_2(DP_{673})$/P25. The apparent quantum yield for the formation of **2** was calculated using the equation $\Phi_{AQY} = (Y_{vis} - Y_{dark})$/(number of photons entering the reaction vessel) × 100%, where Y_{vis} and Y_{dark} are the amounts of **2** formed under light irradiation and dark conditions, respectively.

Catalytic Activity. The efficacy of the Au/P25 catalyst for photoreaction was evidenced by the aerobic oxidation of 1-phenylethanol (**1**), which is often used as substrate for aerobic oxidation,[7−9] to give acetophenone (**2**). The reaction was performed by stirring a toluene solution (5 mL) containing **1** (1 mmol) and catalyst (20 mg) under 1 atm O_2. The solution temperature was kept rigorously at 298 ± 0.5 K. Figure 2 summarizes the amounts of **2** formed after 12 h of reaction in the dark (black bars) or under visible-light irradiation (Xe lamp, $\lambda > 450$ nm, white bars). Notably, both reaction conditions selectively produced **2**, where the mass balance of **1** and **2** was >99% and no byproducts were detected. In addition, the

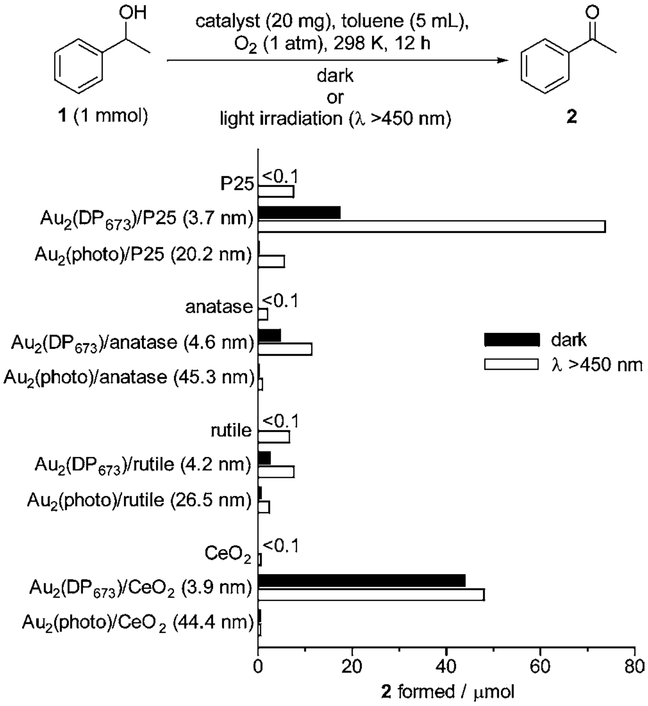

Figure 2. Amounts of **2** formed during aerobic oxidation of **1** with respective catalysts (black) in the dark or (white) under visible-light irradiation ($\lambda > 450$ nm; light intensity at 450−800 nm, 16.8 mW cm^{-2}). The d_{Au} values for the catalysts are given in parentheses. The detection limit of **2** was 0.02 μmol (4 μM), and the range of calibration was 0.004−200 mM.

absence of O_2 scarcely promoted the reaction. With bare P25, no reaction occurred in the dark, and light irradiation produced <10 μmol of **2**. In contrast, $Au_2(DP_{673})/P25$ in the dark produced 17 μmol of **2** as a result of the high activity of the small Au particles.[13−15] Light irradiation further enhanced the reaction: 74 μmol of **2** was produced, which is more than 4 times that obtained from the dark reaction. This suggests that visible-light irradiation of the Au/P25 catalyst indeed enhances the reaction.

An anatase or rutile TiO_2 support was ineffective for reaction: the $Au_2(DP_{673})$/anatase and $Au_2(DP_{673})$/rutile catalysts produced only ca. 10 μmol of **2** even under light irradiation. Large Au particles were also ineffective for reaction: the Au_2(photo)/anatase, Au_2(photo)/rutile, and Au_2(photo)/P25 catalysts, which were prepared by a photodeposition method,[21] contained Au particles with d_{Au} = 45.3, 26.5, and 20.2 nm, respectively,[23] and were inactive under both sets of reaction conditions. A semiconductor CeO_2 support (JRC-CEO-3; 20 nm; 82 m^2 g^{-1}) was also ineffective. The dark activity of $Au_2(DP_{673})/CeO_2$ (d_{Au} = 3.9 nm) was very high because of the enhanced dehydrogenation of **1** on the basic CeO_2 surface,[5] but the activity was scarcely enhanced by light irradiation. In addition, $Au_2(photo)/CeO_2$ (d_{Au} = 44.4 nm) was inactive under both sets of conditions. These data clearly suggest that small Au particles loaded on P25 TiO_2 specifically show high catalytic activity under visible-light irradiation. As shown in Figure 1a, the SPR intensities of the catalysts are inconsistent with their activities, although early reports suggested the association.[21,22] These data indicate that the combination of small Au particles and the mixed anatase/rutile TiO_2 support is crucial for high activity.

Electron Transfer from Plasmon-Activated Au Particles. The enhanced aerobic oxidation on Au/P25 by visible-light irradiation is initiated by the plasmon activation of Au particles.[17] Action spectrum analysis confirmed this (Figure 1b): the SPR band of $Au_2(DP_{673})/P25$ correlates well with the apparent quantum yield (Φ_{AQY}) for the formation of **2**. As shown in Scheme 1, the photoactivated Au particles transfer e^- to TiO_2, and e^- is consumed by the reduction of O_2 there. This was confirmed by electron spin resonance (ESR) analysis of the catalysts at 77 K after treatment with O_2 at room temperature in the dark or under visible-light irradiation. As shown in Figure 3a (gray), bare P25 treated in the dark was ESR-silent. In contrast, visible-light irradiation (black) created very weak signals attributable to superoxide-type oxygen anions (O_2^-; g_{xx} = 2.003, g_{yy} = 2.009, g_{zz} = 2,025),[24] which is formed by the reduction of O_2 on the photoexcited TiO_2 surface.[25,26] As shown in Figure 3b, $Au_2(DP_{673})/P25$ in the dark was also ESR-silent, but visible-light irradiation created very strong signals (g_{xx}' = 2.002, g_{yy}' = 2.004, g_{zz}' = 2.008) attributable to peroxo-type oxygen anions ($O{-}O^-$).[27] In contrast, as shown in Figure 3c,d, the $Au_2(DP_{673})$/anatase and $Au_2(DP_{673})$/rutile catalysts, which were inactive for photoreaction (Figure 2), scarcely showed these signals, although their d_{Au} values are similar to that for $Au_2(DP_{673})/P25$. This suggests that the $O{-}O^-$ species do not form on the Au surface but do form on the P25 TiO_2 surface and that, as shown in Scheme 1, plasmon activation of Au particles transfers e^- to P25 TiO_2 and promotes O_2 reduction there.

The formation of $O{-}O^-$ species, not superoxide (O_2^-), is rationalized by O_2 reduction at the Au/TiO_2 interface. The structure of the oxygen anion depends strongly on its local environment.[24] In the present case, the e^- transfer might occur at the Au/TiO_2 interface. The formed oxygen anion therefore probably interacts with a residual positive charge on the Au particles, as shown in Figure 3b, and produces the peroxo-type anion. It must be noted that, as shown in Figure 3b (green), the Au/P25 catalyst, when treated with O_2 at 363 K in the dark, did not show the $O{-}O^-$ signal. This indicates that light-to-heat conversion,[28] even if it occurs on the photoactivated Au particles, does not promote O_2 reduction. These findings strongly support the e^- transfer from photoactivated Au particles to TiO_2 and subsequent O_2 reduction on the TiO_2 surface (Scheme 1).

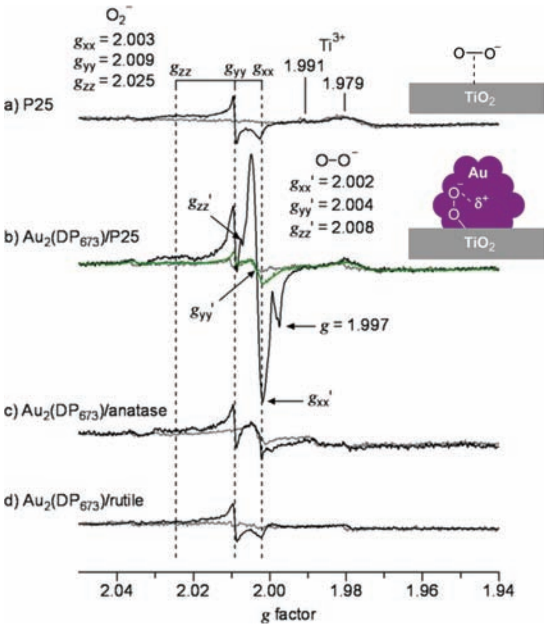

Figure 3. ESR spectra of the catalysts. The catalysts were treated with 20 Torr O_2 (gray) in the dark or (black) under visible-light irradiation at 298 K or (green) in the dark at 363 K. After evacuation, the samples were measured at 77 K. The g = 1.997 signal (spectrum b) is assigned to e^- at the lattice trapping site of TiO_2.[26]

Effects of Size and Location of the Au Particles. The amount of Au loaded strongly affects the activity of the plasmonic photocatalysis. Figure 4a shows the results of aerobic oxidation using $Au_x(DP_{673})/P25$ catalysts with different Au loadings [x wt % = $Au/(Au + TiO_2) \times 100\%$]. The activity increased with the Au loading (∼2 wt %) but decreased at higher loadings (>3 wt %); the activity of the Au_5 catalyst under visible-light irradiation was similar to the dark activity. This suggests that Au loadings of 2−3 wt % show the highest catalytic activity. The d_{Au} values for the $Au_{0.5}$, Au_2, Au_3, and Au_5 catalysts were 2.4, 3.7, 4.9, and 7.8 nm, respectively, implying that small Au particles with d_{Au} < 5 nm are active for reaction.

To clarify further the effect of the Au particle size on the activity, $Au_2(DP_y)/P25$ catalysts prepared at different calcination temperatures y (in K) were used for the reaction. As shown in Figure 4b, the d_{Au} values for the DP_{473}, DP_{573}, DP_{673}, DP_{773}, and DP_{873} catalysts were 3.3, 3.4, 3.7, 7.6, and 8.3 nm, respectively. The DP_{773} and DP_{873} catalysts with larger Au particles showed much lower activities than DP_{673}, suggesting that Au particles with d_{Au} > 5 nm are indeed inactive. In contrast, d_{Au} for DP_{473} was similar to that for DP_{673}, but the activity was much lower. This indicates that the calcination temperature as well as the size of the Au particles affects the activity for the plasmonic reaction.

The active sites for the plasmonic reaction on Au/P25 are the Au particles (d_{Au} < 5 nm) located at the anatase/rutile

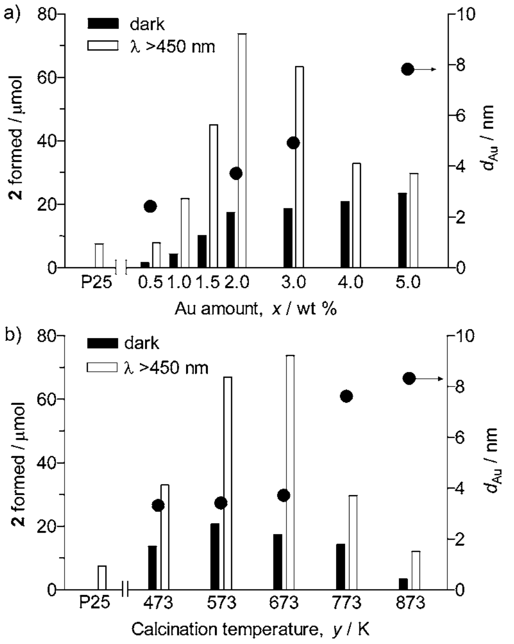

Figure 4. Amounts of **2** formed during oxidation of **1** at 298 K with (a) $Au_x(DP_{673})$/P25 and (b) $Au_2(DP_y)$/P25 catalysts. The reaction conditions were identical to those in Figure 2.

interfaces. The difference in the activities of catalysts prepared at the different calcination temperatures 473−673 K (Figure 4b) is explained by the migration of Au particles on the P25 TiO_2 surface during calcination, as clarified by Akita et al.[29] During the preparation of Au particles on P25 TiO_2 by the DP method, calcination at ≥423 K fully reduces the Au species and produces Au particles.[30] As schematically shown in Figure 5a, upon calcination at 473 K, Au particles form mainly on the rutile surface because a number of oxygen vacancies act as the crystal nucleation sites.[31] In contrast, calcination at higher temperature promotes the migration of Au particles, and they are stabilized at the anatase/rutile interface (Figure 5b).[29] The TEM image of $Au_2(DP_{473})$/P25 (Figure 5a) shows Au particles located on the surface of the TiO_2 particles, but that of $Au_2(DP_{673})$/P25 (Figure 5b) shows Au particles located at the interfaces of the TiO_2 particles. As shown in Figure 6, the HRTEM images of $Au_2(DP_{673})$/P25 clearly show the Au particles located at the anatase/rutile interface and well-defined contact surfaces for the Au/anatase/rutile phases. X-ray photoelectron spectroscopy (XPS) of the catalysts further confirmed this. As shown in Figure 7, the binding energy for the Au $4f_{7/2}$ orbital of $Au_2(DP_{673})$/rutile (82.58 eV) is much lower than that of $Au_2(DP_{673})$/anatase (82.71 eV) because of the strong binding of Au with the oxygen vacancies on the rutile surface.[31] The binding energy of $Au_2(DP_{473})$/P25 (82.60 eV) is similar to that of $Au_2(DP_{673})$/rutile (82.58 eV), but that of $Au_2(DP_{673})$/P25 (82.65 eV) is much higher. These data indicate that, as reported,[29] Au particles prepared at higher calcination temperatures are mainly located at the anatase/rutile interfaces and behave as the active sites for the plasmonic reaction.

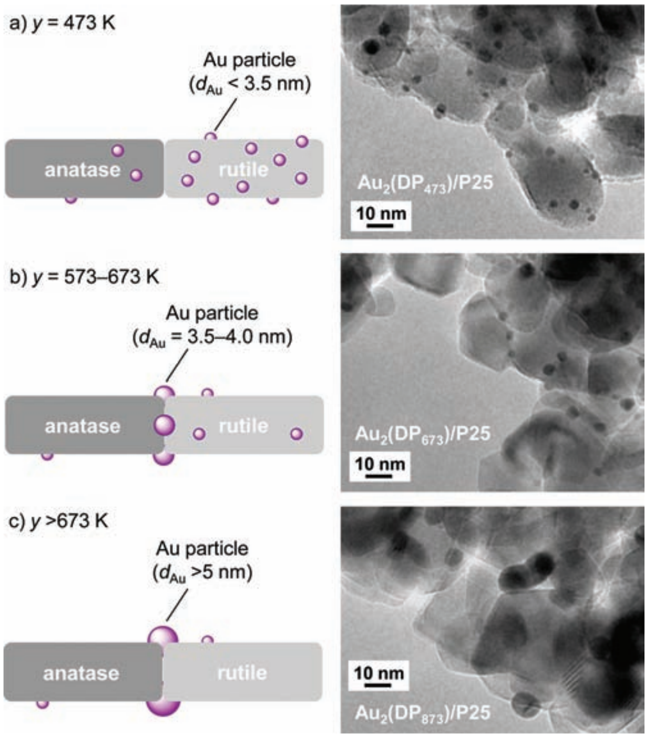

Figure 5. Effect of calcination temperature on the location and size of Au particles on P25 TiO_2[29] and typical TEM images for $Au_2(DP_y)$/P25 catalysts. More images are shown in Figure S3 in the Supporting Information.

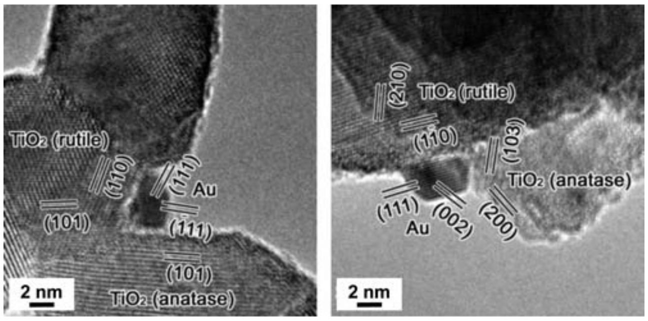

Figure 6. HRTEM images of $Au_2(DP_{673})$/P25. More images are shown in Figure S4 in the Supporting Information.

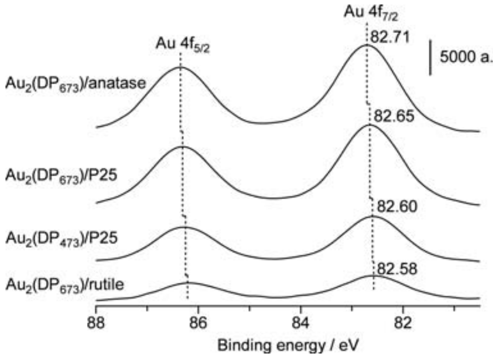

Figure 7. XPS results for the catalysts.

Mechanism for Plasmonic Catalysis. $Au_2(DP_{673})$/anatase and $Au_2(DP_{673})$/rutile, which are inactive for the plasmonic reaction, show almost no ESR signals for $O{-}O^-$ species (Figure 3c and d). This indicates that O_2 is scarcely reduced on these TiO_2 surface. As reported,[32] O_2 reduction by the conduction-band e^- on the rutile surface is inefficient because of the low affinity between the surface and O_2.[33] This may result in inefficient O_2 reduction on the rutile catalyst. In contrast, anatase is active for O_2 reduction.[34] The almost complete absence of O_2 reduction on the anatase catalyst is probably due to the weak binding between Au and anatase, as evidenced by the XPS analysis (Figure 7). This may suppress e^- transfer from photoactivated Au particles to anatase. Efficient O_2 reduction on the Au/P25 catalyst is explained by the following mechanism, as summarized in Scheme 2: (a) plasmon activation of Au particles transfers e^- to the tightly bound rutile; (b) e^- is then transferred to well-conjugated anatase; and, (c) O_2 is reduced there by e^- (formation of O–O^- species). The e^- transfer from rutile to anatase is thermodynamically unfavorable because the conduction band potential (E_{CB}) of rutile (−0.05 V vs NHE) is more positive than the E_{CB} of anatase (−0.25 V).[35] However, it is allowed by a negative shift of the rutile E_{CB} (Scheme 2b);[34,36,37] the e^- injection from Au particles to rutile accumulates e^- in its conduction band and results in the negative shift of E_{CB}. This promotes consecutive e^- transfer from the Au particles to rutile and then to anatase and efficient O_2 reduction on the anatase surface. Therefore, the Au/anatase/rutile joint active site promotes the plasmonic reaction.

Scheme 2. Proposed Mechanism for Aerobic Oxidation of Alcohol on the Au/P25 Catalyst under Visible-Light Irradiation

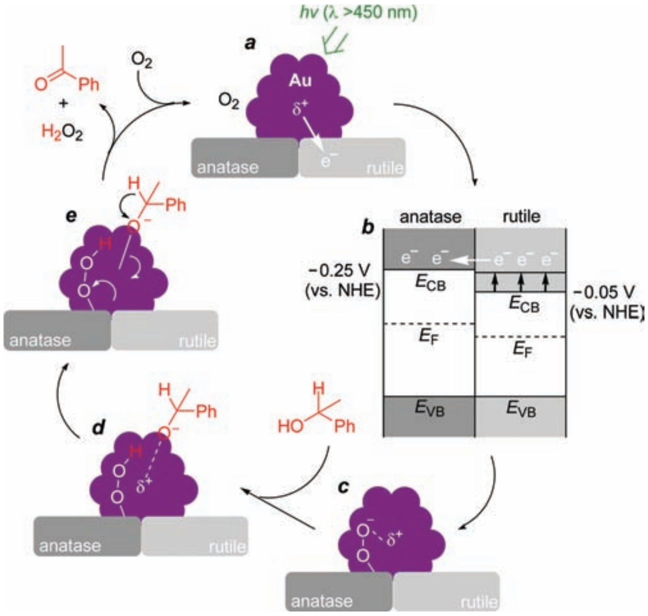

As shown in Figure 4b, the $Au_2(DP_y)$/P25 catalysts prepared at higher calcination temperatures (>673 K) show decreased activity. As shown in Figure 5c, calcination at >673 K produces larger Au particles via the sintering of particles.[29] The formation of larger Au particles decreases the number of joint active sites, thus resulting in an activity decrease.[38] Aerobic oxidation at the joint active site is explained as in Scheme 2. The O–O^- species (c) probably attracts the H atom of the alcohol while the positive charge on Au adsorbs the alcohol, producing a Au–alcoholate species (d).[39,40] Subsequent removal of the H atom from this species (e) produces the carbonyl product.

Aerobic Oxidation by Exposure to Sunlight. The reaction temperature strongly affects the activity of the plasmonic reaction. Figure 8 shows the results of aerobic oxidation with $Au_2(DP_{673})$/P25 at different temperatures. The dark activity increased with increasing temperature.[8] In contrast, under visible-light irradiation, the highest activity was obtained at 298 K, and the activity decreased at lower or higher temperature. Two factors may affect the plasmonic catalysis. The activity decrease at higher temperature is due to the positive E_{CB} shift of TiO_2, as usually observed for dye-sensitized TiO_2:[41] e^- transfer within TiO_2 decreases with increasing in temperature at 293–333 K. In the present case, this positive E_{CB} shift probably suppresses the e^- transfer from rutile to anatase and/or the O_2 reduction on the anatase surface, resulting in the activity decrease at higher temperature. This means that lower temperature is favorable for plasmonic catalysis. The activity, however, decreases for $T < 298$ K. This is probably due to the decrease in electron conductivity of Au particles with decreasing temperature (<333 K).[42] This may suppress the e^- injection from Au particles to TiO_2 and decrease the catalytic activity. These two factors affect the activity of plasmonic catalysis at lower or higher temperature.

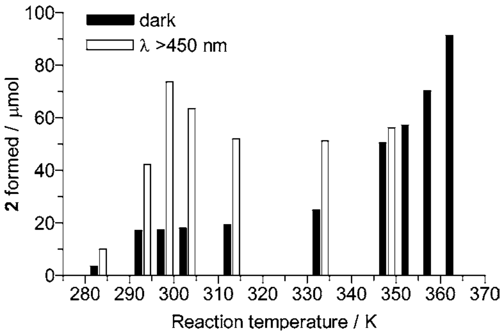

Figure 8. Effect of reaction temperature on the amount of **2** formed during oxidation of **1** with $Au_2(DP_{673})$/P25. The reaction conditions were identical to those in Figure 2.

These data suggest that visible-light irradiation at around room temperature are the conditions suitable for maximizing the activity of plasmonic catalysis. Sunlight exposure is a typical case. Table 1 summarizes the results of aerobic oxidation of alcohols using the $Au_2(DP_{673})$/P25 catalyst under sunlight, where the solution temperature during exposure was 300–303 K. Exposure to sunlight successfully promoted selective oxidation of alcohols to carbonyl compounds in high yields (79–99%), and the yields were higher than those obtained under dark conditions at 303 K. These results suggest that the plasmonic catalysis is successfully activated by sunlight and promotes aerobic oxidation.

■ CONCLUSION

We have clarified that Au nanoparticles with diameters of <5 nm located at the interface of anatase/rutile TiO_2 particles behave as active sites for plasmonic photocatalysis under visible-light irradiation. The joint active site consisting of Au/anatase/rutile phases facilitates smooth e^- transfer from the photoactivated Au particles to TiO_2 and efficient O_2 reduction. Sunlight activation of the catalyst successfully promotes aerobic oxidation of alcohols at ambient temperature. The catalyst architecture clarified here for active plasmonic photocatalysis may contribute to the design of more efficient catalysts driven by visible light and may open a new strategy for selective organic transformations by sunlight.

■ EXPERIMENTAL SECTION

Preparation of Catalysts. $Au_x(DP_y)$/P25 catalysts [x = 0.5, 1, 2, 3, 4, 5; y = 473, 573, 673, 773, 873] were prepared by the following

Table 1. Effect of Sunlight Exposure on the Aerobic Oxidation of Alcohols Using the $Au_2(DP_{673})/P25$ Catalyst[a]

entry	alcohol	sunlight[b]	conv. / %[c]	product	yield / %[d]
1	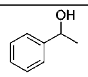	+	79	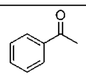	79
2		−	30		30
3[e]	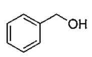	+	85	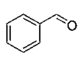	79
4		−	25		22
5	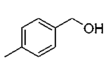	+	>99	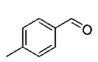	99
6		−	31		30
7[f]	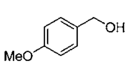	+	>99	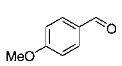	90
8		−	40		37
9	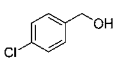	+	88	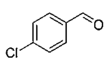	87
10		−	16		15
11	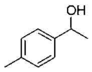	+	83	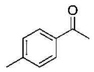	82
12		−	61		58
13[g]	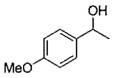	+	>99	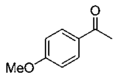	>99
14[g]		−	42		42
15[h]	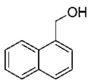	+	>99	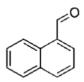	92
16		−	62		51
17	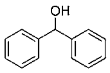	+	81	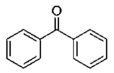	80
18		−	51		50

[a] Reaction conditions: toluene (5 mL), alcohol (10 μmol), catalyst (20 mg), O_2 (1 atm), exposure time (4 h). The light intensity at 300−800 nm was 11.5 mW cm^{-2}, which involves only ca. 2% <400 nm light. The solution temperature during exposure was 300−303 K. [b] The dark reaction (−) was performed at 303 K. [c] (Alcohol converted)/(initial amount of alcohol) × 100%. [d] (Product formed)/(initial amount of alcohol) × 100%. [e] Benzoic acid (0.4 μmol) was formed. [f] *p*-Methoxybenzoic acid (0.4 μmol) was formed. [g] Catalyst (10 mg). [h] 1-Napthoic acid (0.5 μmol) was formed.

procedure: P25 (1.0 g) was added to water (50 mL) containing $HAuCl_4 \cdot 4H_2O$ (11.2, 22.9, 45.8, 68.7, 91.6, or 114.5 mg). The solution pH was adjusted to ca. 7 with 1 mM NaOH, and the solution was stirred at 353 K for 3 h. The particles were recovered by centrifugation, washed thoroughly with water, and dried at 353 K for 12 h. The powders were calcined under air with a heating rate of 2 K min^{-1} and a holding time of 2 h at the designated temperature. $Au_2(DP_{673})$/anatase, $Au_2(DP_{673})$/rutile, and $Au_2(DP_{673})/CeO_2$ were prepared in a similar manner. X-ray fluorescence (XRF) analysis indicated that only a trace amount of Cl^- (<10 ppm) remained in the catalysts.

Au_2(photo)/P25 was prepared as follows: TiO_2 (1.0 g) was added to a water/MeOH mixture (1:1 v/v, 50 mL) containing $HAuCl_4 \cdot 4H_2O$ (45.8 mg) within a Pyrex glass tube (φ, 25 mm; capacity, 100 mL), and the tube was sealed with a rubber septum cap. The particles were dispersed by ultrasonication for 5 min, and Ar gas was bubbled through the solution for 15 min. The tube was photoirradiated at $\lambda > 320$ nm for 2 h at 298 K with magnetic stirring using a 300 W Hg lamp (Eikohsha Co.)[43] and then filtered through a 5 wt % $CuSO_4$ solution. The powders were recovered by centrifugation, washed thoroughly with water, and dried at 353 K for 12 h. Au_2(photo)/anatase and Au_2(photo)/rutile were prepared in a similar manner. Au_2(photo)/CeO_2 was prepared by photoirradiation (2 h, 298 K) of CeO_2 (1.0 g) suspended in water (50 mL) containing $HAuCl_4 \cdot 4H_2O$ (45.8 mg) and citric acid monohydrate (70.5 mg). XRF analysis indicated that only a trace amount of Cl^- (<10 ppm) remained in the catalysts.

Reaction Procedure. The catalyst (20 mg) was added to toluene (5 mL) containing the alcohol within a Pyrex glass tube (φ, 10 mm; capacity, 20 mL), and the tube was sealed with a rubber septum cap. The catalyst was dispersed well by ultrasonication for 5 min, and O_2 was bubbled through the solution for 5 min. The tube was immersed in a temperature-controlled water bath (298 ± 0.5 K) and photoirradiated at $\lambda > 450$ nm with magnetic stirring using a 2 kW Xe lamp (USHIO Inc.)[44] filtered through a CS3-72 glass (Kopp Glass Inc.); the light intensity at 450−800 nm was 16.8 mW cm^{-2} (Figure S6 in the Supporting Information). Sunlight reactions were performed on Oct 4, 2011, from 10:00 to 14:00 at the top of the laboratory building (north latitude 34.7°, east longitude 135.5°; see Figure S7 in the Supporting Information). The light intensity at 300−800 nm was 11.5 mW cm^{-2} (Figure S6 in the Supporting Information). The highest solution temperature during exposure was 303 K, and the dark experiments were carried out at 303 K. After the reactions, the catalyst was recovered by centrifugation, and the solution was analyzed by GC−FID (Shimadzu GC-2040) equipped with a DB-17 capillary column (Agilent Technologies, 30 m × 0.250 mm × 0.25 μm). The substrate and product concentrations were calibrated with authentic samples. The analysis was performed at least three times, and the errors were ±0.2%. Products were identified using a GC−MS system (Shimadzu GCMS-QP5050A).

Action Spectrum Analysis. The photoreaction was carried out with a toluene solution (2 mL) containing **1** (0.4 mmol) and the $Au_2(DP_{673})/P25$ catalyst (8 mg) within a Pyrex glass tube. After ultrasonication and O_2 bubbling, the solution was photoirradiated using a 2 kW Xe lamp whose light was monochromatized by band-pass glass filters (Asahi Techno Glass Co.). The full-width at half-maximum (fwhm) of the light was 11−16 nm. The number of photon entering the reaction vessel was determined with a spectroradiometer (USR-40, USHIO Inc.).

ESR Measurements. The spectra were recorded in the X-band using a Bruker EMX-10/12 spectrometer with a 100 kHz magnetic field modulation at a microwave power of 10.0 mW.[45] The magnetic field was calibrated using 1,1′-diphenyl-2-picrylhydrazyl (DPPH) as a standard. The catalyst (20 mg) was placed in a quartz ESR tube, which was evacuated at 423 K for 3 h and cooled to room temperature. O_2 (20 Torr) was introduced into the tube and kept for 10 min. The tube was photoirradiated at 298 K using a Xe lamp at λ >450 nm. The tube was then evacuated for 10 min to remove excess O_2 and analyzed at 77 K.

Analysis. Total amounts of Au in the catalysts were determined using an inductively coupled argon plasma atomic emission spectrometer (ICAP-AES; SII Nanotechnology, SPS 7800) after dissolution of the catalysts in aqua regia. TEM observations were carried out using an FEI Tecnai G2 20ST analytical electron microscope operated at 200 kV. XPS analysis was performed using a JEOL JPS-9000MX spectrometer with Mg Kα radiation as the energy source. Diffuse-reflectance UV−vis spectra were measured on an UV−vis spectrophotometer (Jasco V-550 with Integrated Sphere Apparatus ISV-469) using $BaSO_4$ as a reference. XRF analysis was carried out on an X-ray fluorescence spectrometer (SEA2110, Seiko Instruments Inc.).

■ ASSOCIATED CONTENT

Ⓢ Supporting Information

Catalyst properties (Table S1), TEM images and size distribution of Au particles (Figure S1), diffuse-reflectance UV−vis spectra of catalysts (Figure S2), typical TEM images of $Au_2(DP)_y/P25$ (Figure S3), HRTEM images of $Au_2(DP_{673})/P25$ (Figure S4), XRD patterns of catalysts (Figure 5), spectral irradiance of the light source (Figure S6), and an image of the sunlight reaction (Figure S7). This material is available free of charge via the Internet at http://pubs.acs.org.

■ AUTHOR INFORMATION

Corresponding Author

shiraish@cheng.es.osaka-u.ac.jp

Notes

The authors declare no competing financial interest.

■ ACKNOWLEDGMENTS

This work was supported by a Grant-in-Aid for Scientific Research (23360349) from the Ministry of Education, Culture, Sports, Science and Technology (MEXT), Japan. D.T. thanks the Japan Society for Promotion of Science (JSPS) for a Research Fellowship for Young Scientists.

■ REFERENCES

(1) Haruta, M. *Nature* **2005**, *437*, 1098−1099.

(2) Herzing, A. A.; Kiely, C. J.; Carley, A. F.; Landon, P.; Hutchings, G. J. *Science* **2008**, *321*, 1331−1335.

(3) Pina, C. D.; Falletta, E.; Prati, L.; Rossi, M. *Chem. Soc. Rev.* **2008**, *37*, 2077−2095.

(4) Gajan, D.; Guillois, K.; Delichère, P.; Basset, J. M.; Candy, J. P.; Caps, V.; Copéret, C.; Lesage, A.; Emsley, L. *J. Am. Chem. Soc.* **2009**, *131*, 14667−14669.

(5) Abad, A.; Concepcion, P.; Corma, A.; Garcia, H. *Angew. Chem., Int. Ed.* **2005**, *44*, 4066−4069.

(6) Pratti, L.; Rossi, M. *J. Catal.* **1998**, *176*, 552−560.

(7) Ishida, T.; Nagaoka, M.; Akita, T.; Haruta, M. *Chem.—Eur. J.* **2008**, *14*, 8456−8460.

(8) Abad, A.; Corma, A.; Garcia, H. *Chem.—Eur. J.* **2008**, *14*, 212−222.

(9) Mitsudome, T.; Noujima, A.; Mizugaki, T.; Jitsukawa, K.; Kaneda, K. *Adv. Synth. Catal.* **2009**, *351*, 1890−1896.

(10) Corma, A.; Domine, M. E. *Chem. Commun.* **2005**, 4042−4044.

(11) Hughes, M. D.; Xu, Y.-J.; Jenkins, P.; McMorn, P.; Landon, P.; Enache, D. I.; Carley, A. F.; Attard, G. A.; Hutchings, G. J.; King, F.; Stitt, E. H.; Johnston, P.; Griffin, K.; Kiely, C. J. *Nature* **2005**, *437*, 1132−1135.

(12) Turner, M.; Golovko, V. B.; Vaughan, O. P. H.; Abdulkin, P.; Berenguer-Murcia, A.; Tikhov, M. S.; Johnson, B. F. G.; Lambert, R. M. *Nature* **2008**, *454*, 981−984.

(13) Haruta, M. *Catal. Today* **1997**, *36*, 153−166.

(14) Valden, M.; Lai, X.; Goodman, D. W. *Science* **1998**, *281*, 1647−1650.

(15) Haruta, M.; Date, M. *Appl. Catal., A* **2001**, *222*, 427−437.

(16) Jain, P. K.; Huang, X.; El-Sayed, I. H.; El-Sayed, M. A. *Acc. Chem. Res.* **2008**, *41*, 1578−1586.

(17) Tian, Y.; Tatsuma, T. *J. Am. Chem. Soc.* **2005**, *127*, 7632−7637.

(18) Grätzel, M. *Nature* **2001**, *414*, 338−344.

(19) Linsebigler, A. L.; Lu, G.; Yates, J. T. Jr. *Chem. Rev.* **1995**, *95*, 735−738.

(20) Primo, A.; Corma, A.; Garcia, H. *Phys. Chem. Chem. Phys.* **2011**, *13*, 886−910.

(21) Kowalska, E.; Mahaney, O. O. P.; Abe, R.; Ohtani, B. *Phys. Chem. Chem. Phys.* **2010**, *12*, 2344−2355.

(22) Tanaka, A.; Hashimoto, K.; Kominami, H. *Chem. Commun.* **2011**, *47*, 10446−10448.

(23) As shown in Figure S1 in the Supporting Information, the photodeposition method creates Au particles with a wide size distribution (ca. ±40 nm), as observed for related materials (see refs 20−22). In contrast, the DP method creates Au particles with size distributions of ca. ±5 nm (see refs 13 and 15).

(24) Anteliff, K. L.; Murphy, D. M.; Griffiths, E.; Giamello, E. *Phys. Chem. Chem. Phys.* **2003**, *5*, 4306−4316.

(25) Anpo, M.; Che, M.; Fubini, B.; Garrone, E.; Giamello, E.; Paganini, M. C. *Top. Catal.* **1999**, *8*, 189−198.

(26) Rajh, T.; Ostafin, A. E.; Micic, O. I.; Tiede, D. M.; Thurnauer, M. C. *J. Phys. Chem.* **1996**, *100*, 4538−4545.

(27) Chowdhury, B.; Bravo-Suarez, J. J.; Mimura, N.; Lu, J.; Bando, K. K.; Tsubota, S.; Haruta, M. *J. Phys. Chem. B* **2006**, *110*, 22995−22999.

(28) Chen, X.; Zhu, H.-Y.; Zhao, J.-C.; Zheng, Z.-F.; Gao, X.-P. *Angew. Chem., Int. Ed.* **2008**, *47*, 5353−5356.

(29) Akita, T.; Lu, P.; Ichikawa, S.; Tanaka, K.; Haruta, M. *Surf. Interface Anal.* **2001**, *31*, 73−78.

(30) Zanella, R.; Giorgio, S.; Shin, C.-H.; Henry, C. R.; Louis, C. *J. Catal.* **2004**, *222*, 357−367.

(31) Chen, M.; Goodman, W. *Acc. Chem. Res.* **2006**, *39*, 739−746.

(32) Ohno, T.; Sarukawa, K.; Matsumura, M. *J. Phys. Chem. B* **2001**, *105*, 2417−2420.

(33) Smith, W. R.; Forg, D. G. *J. Phys. Chem.* **1965**, *69*, 3587−3592.

(34) Ohno, T.; Tokieda, K.; Higashida, S.; Matsumura, M. *Appl. Catal., A* **2003**, *244*, 383−391.

(35) Maruska, H. P.; Ghosh, A. K. *Sol. Energy* **1978**, *20*, 443−458.

(36) Dunn, W. W.; Aikawa, Y.; Bard, A. J. *J. Am. Chem. Soc.* **1981**, *103*, 3456−3459.

(37) Fujii, M.; Kawai, T.; Kawai, S. *Chem. Phys. Lett.* **1984**, *106*, 517−522.

(38) The anatase-to-rutile phase transition of P25 upon calcination at higher temperature is not the major factor causing decreased photocatalytic activity. As shown in Figure S5 in the Supporting Information), XRD patterns indicated the anatase/rutile ratios of $Au_2(DP_{673})$/P25 and $Au_2(DP_{773})$/P25 catalysts to be 83:17, which is similar to that of pure P25, although the increased amount of rutile in $Au_2(DP_{873})$/P25 as a result of the phase transition changed the ratio to 73:27. As shown in Figure 4b, $Au_2(DP_{773})$/P25 showed lower activity than $Au_2(DP_{673})$/P25, even though their anatase/rutile ratios are similar. This indicates that the phase transition of P25 is not the major factor causing the lower photocatalytic activity of the catalysts prepared at higher calcination temperatures.

(39) It is well-known that in the aerobic oxidation of alcohols with supported Au catalysts under dark conditions, the interaction between the alcohol and the surface of the support is very important for oxidation activity. In that case, basic supports such as CeO_2 accelerate the deprotonation of alcohols and promote the formation of Au−alcoholate species (see refs 5 and 8). As shown in Table S1 in the Supporting Information, the point of zero charge of $Au_2(DP_{673})$/P25 was determined to be 5.9, suggesting that the P25 surface is weakly acidic and less active for the deprotonation of alcohols. This means that the interaction between the alcohol and the P25 surface scarcely affects the plasmonic catalysis.

(40) A similar mechanism for the formation of Au−alcoholate species was proposed by Ishida et al. (ref 7). They reported that Au clusters supported on porous coordination polymers (PCPs) showed very high activity for aerobic oxidation of alcohols under dark conditions, even though the PCP support is weakly acidic. This high activity was explained by successful O_2 activation on the Au clusters due to the electronic interaction with the PCP support. This produces the peroxo-type oxygen anion and positive charge on the Au clusters and promotes the formation of Au−alcoholate species, similar to our system (c → d in Scheme 2).

(41) O'Regan, B. C.; Durrant, J. R. *J. Phys. Chem. B* **2006**, *110*, 8544−8547.

(42) Terrill, R. H.; Postlewaite, T. A.; Chen, C.; Poon, C.-D.; Terzis, A.; Chen, A.; Hutchison, J. E.; Clark, M. R.; Wignall, G.; Londono, J. D.; Superfine, R.; Falvo, M.; Johnson, C. S. Jr.; Samulski, E. T.; Murray, R. W. *J. Am. Chem. Soc.* **1995**, *117*, 12537−12548.

(43) Shiraishi, Y.; Saito, N.; Hirai, T. *J. Am. Chem. Soc.* **2005**, *127*, 8304−8306.

(44) Shiraishi, Y.; Sugano, Y.; Tanaka, S.; Hirai, T. *Angew. Chem., Int. Ed.* **2010**, *49*, 1656−1660.

(45) Shiraishi, Y.; Saito, N.; Hirai, T. *J. Am. Chem. Soc.* **2005**, *127*, 12820−12822.